

# Zeolite Structure Direction by Simple Bis(methylimidazolium) Cations: The Effect of the Spacer Length on Structure Direction and of the Imidazolium Ring Orientation on the $^{19}\text{F}$ NMR Resonances

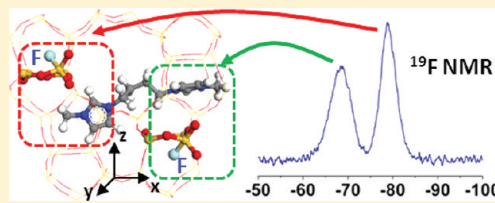
Alex Rojas,<sup>†</sup> Luis Gómez-Hortigüela,<sup>‡</sup> and Miguel A. Camblor<sup>\*,†</sup>

<sup>†</sup>Instituto de Ciencia de Materiales de Madrid (ICMM-CSIC), Sor Juana Inés de la Cruz 3, Cantoblanco 28049, Madrid, Spain

<sup>‡</sup>Instituto de Catálisis y Petroleoquímica (ICP-CSIC), Marie Curie 2, Cantoblanco 28049, Madrid, Spain

## S Supporting Information

**ABSTRACT:** A series of doubly charged structure-directing agents based on two methylimidazolium moieties linked by a linear bridge of  $n = 3, 4, 5$ , or 6 methylene groups has been used in the synthesis of pure silica zeolites in the presence of fluoride. All of them yielded zeolite TON while only the one with  $n = 4$  was able to produce also zeolite MFI at highly concentrated conditions. In this MFI zeolite, two distinct  $^{19}\text{F}$  MAS NMR resonances with about equal intensity were observed, indicating two different chemical environments for occluded fluoride. With the singly charged 1-ethyl-3-methylimidazolium cation, which can be formally considered as the “monomer” of the bis-imidazolium cation with  $n = 4$ , TON and MFI were also obtained, and again two  $^{19}\text{F}$  MAS NMR resonances now with largely dissimilar intensities were observed in MFI. Molecular mechanics simulations support a commensurate structure-direction effect for  $n = 4$  in MFI, with each imidazolium ring, in two different orientations, sitting close to the  $[4^15^26^2]$  cage. Periodic DFT calculations suggest that F in MFI resides always in the  $[4^15^26^2]$  cages, with the different  $^{19}\text{F}$  resonances observed being due to the different orientation of the closest imidazolium ring.



## INTRODUCTION

Structure direction<sup>1,2</sup> by organic species plays a central role in the development of new zeolite structures and compositions. In addition to other effects typically intervening in the crystallization of zeolites, the organic structure-directing agent (SDA) usually ends up filling the zeolite voids providing a stabilization energy that may help the zeolite nucleate and grow. The inorganic–organic host–guest matching may range from a loose pore filling, leading to unspecific structure direction, to a close geometric fitting, providing a more robust and specific effect.<sup>2,3</sup> Despite the frequent cationic nature of organic SDAs, electrostatic interactions are generally considered to contribute to a lesser extent in stabilizing the zeolite frameworks than long-range van der Waals contacts.<sup>1,4</sup> However, recent studies on a pure silica zeolite with the ITW Framework Type Code<sup>5</sup> containing 1,3,4-trimethylimidazolium cations and fluoride anions supported that, in that case, a significant stabilization of the pure silica framework is provided by host–guest charge transfer, in addition to van der Waals interactions.<sup>6,7</sup>

A number of studies have reported on the use as SDA of multicharged organic species containing somewhat bulky cationic moieties linked by flexible bridges of varying length acting as spacers. This strategy was pioneered by Daniels and co-workers,<sup>8</sup> who used quaternary ammonium polymers based on the 1,4-diazabicyclo[2.2.2]octane with linear alkane bridges of varying length as spacers. Later on, several works focused on polymethylene-bis(trimethylammonium) diquatary compounds, “diquats”,  $(\text{CH}_3)_3\text{N}^+(\text{CH}_2)_n\text{N}^+(\text{CH}_3)_3$ , reporting the

formation of EUO for  $n = 5$ ,<sup>9,10</sup> and NEI for  $n = 10$ .<sup>11</sup> This prompted Moini and co-workers to investigate the effect of systematically varying the length of the spacers in this series of diquats.<sup>12</sup> Under particular synthesis conditions, the diquats with  $n = 5–14$  tended to yield zeolites with one-dimensional pores (MTT, for  $n = 7, 8, 11, 12$  or MTW,  $n = 9, 14$ ), except for specific values of  $n$  that gave two-dimensional or quasi-two-dimensional pore zeolites: EUO ( $n = 5, 6$ ) and NES ( $n = 10$ ).<sup>12</sup> The authors proposed that this specificity was related to the correlation between the pore system of the two-dimensional pore zeolites and the length of the corresponding diquats.<sup>12</sup>

These and other examples using doubly charged SDAs<sup>13,14</sup> refer mainly to synthesis in hydroxide media, and the rationalization of the results are generally based more on space filling considerations than on the effect of cationic charges. This is so because, for aluminosilicates and silicates prepared in hydroxide media, van der Waals interactions may be more important than Coulombic interactions.<sup>1</sup> For these materials, framework anionic charges (either Al, Ga, or connectivity defects), needed for charge balance, may have a range of possible locations (i.e., they generally do not show a very large preference for sitting at specific positions). However, in pure silica zeolites prepared in fluoride media, the cationic charge of the SDA is balanced by occluded fluoride and this anion has been shown to have a relatively large preference for sitting in small cavities.<sup>15</sup> Among those, double four ring cages

Received: November 14, 2011

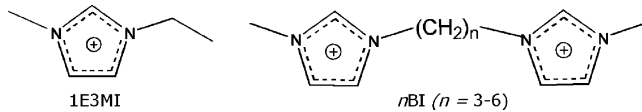
Published: January 24, 2012

(denoted as D4R or [4<sup>6</sup>] cages) seem to be preferred,<sup>16,17</sup> while larger cavities containing some four rings are also frequent. Preferential location of fluoride in small cavities must be accompanied by siting of the cation in larger spaces in its close vicinity and it may even impose ordering on the organic cations.<sup>18,19</sup> Thus, we hypothesized that cation–anion pairings between positive moieties of doubly charged cations and fluoride occluded in small cavities of the silica wall could give rise to specific structure-direction effects when the charges are separated by a length commensurate to the distance between F-containing cages. This has been studied before for polymethylene-bis(quinuclidinium),<sup>20</sup> polymethylene-bis(trimethylammonium),<sup>21</sup> and a series of diquats with different heterocyclic cationic groups,<sup>22</sup> but the discovery of charge transfer effects in ITW prompted us to perform a study with polymethylene-bis(methylimidazolium) molecules.

## EXPERIMENTAL SECTION

**Synthesis of the SDAs.** The organic SDAs used in this work comprise a series of doubly charged cations consisting of two N-methylimidazolium charged moieties spaced by a linear bridge of  $n = 3, 4, 5$ , or  $6$  methylene groups, plus the singly charged N-ethyl-N'-methylimidazolium (Chart 1). The doubly charged SDAs, denoted as

Chart 1. Organic Cations Used in This Work as SDAs



nBI, were synthesized by reaction of 1-methylimidazole with the corresponding linear  $\alpha,\omega$ -dibromoalkane, Br(CH<sub>2</sub>)<sub>n</sub>Br. In a typical synthesis, 11.494 g (0.14 mol) of 1-methylimidazole (Aldrich 98%) was dissolved in 100 mL of chloroform (Aldrich 99%). The linear alkyl bromide (0.07 mol, Fluka 99% for  $n = 3$  or Aldrich 96–99% for  $n = 4–6$ ) was added to the solution, which was kept under magnetic stirring at room temperature for 4 days. The bromide salt was then separated by rotoevaporation. The singly charged 1-ethyl-3-methylimidazolium, denoted 1E3MI, was bought as its chloride salt from Aldrich (>95%).

The <sup>1</sup>H NMR spectra of the SDA salts dissolved in D<sub>2</sub>O or CDCl<sub>3</sub> confirmed that we obtained the different SDAs with acceptable purity (Supporting Information Figure S1). When the spectra were recorded in D<sub>2</sub>O, the moderately acidic H at position 2 (labeled as ‘a’ in Figure S1) of the imidazolium ring eventually showed a reduced relative intensity due to <sup>1</sup>H–<sup>2</sup>H exchange.

The dibromide or chloride salts were converted into the corresponding hydroxides by anion exchange. A total of 0.03 mol of SDA salt was dissolved in water (1 SDA/10 H<sub>2</sub>O weight ratio) and the solution was contacted with 100 mL of exchange resin (Dowex monosphere 550A (OH) anion exchange resin, Aldrich, 1.1 mequiv./1 mL). After 12 h under stirring at room temperature, the hydroxide solution was recovered by filtration, and was concentrated by rotoevaporation under vacuum at 414 K. The final concentration of the hydroxide solution was determined by titration with HCl 0.1 N. The yield of the exchange plus concentration process (final equivalents of hydroxide per 100 starting equivalents of cation) was over 90%.

**Synthesis of Zeolites.** Tetraethylorthosilicate (TEOS, 98%, Aldrich) was hydrolyzed under stirring at room temperature in an aqueous solution of the hydroxide form of the corresponding SDA cation. Some water and all ethanol, produced by the hydrolysis, were eliminated by evaporation, which was monitored by weight loss. The stirring was stopped when the desired H<sub>2</sub>O/SiO<sub>2</sub> ratio was achieved. Then, the required amount of a concentrated aqueous solution of HF (48% Aldrich) was added while stirring with a spatula for 15 min.

The obtained gels were distributed in Teflon lined stainless steel autoclaves which were heated at 423 K while tumbled at 60 rpm.

At different time intervals, the autoclaves were taken out from the oven and quenched with tap water, and the solid products were recovered by filtration and exhaustively washed with water. The final composition of the reaction mixtures was SiO<sub>2</sub>:0.5 ROH:0.5 HF:w H<sub>2</sub>O, and the H<sub>2</sub>O/SiO<sub>2</sub> ratio was varied between 8.5 and 3.5. In the above composition, R stands for an equivalent of the SDA used.

**Characterization.** The recovered solids were identified by powder X-ray diffraction (XRD), recorded in a Bruker D8 Advance diffractometer using Cu K $\alpha$  radiation between 5 and 45° 2θ values. Multi-nuclear magic angle spinning (MAS) NMR spectroscopy of as-made samples were carried out at room temperature on a Bruker AV-400-WB equipment (details are given in the Supporting Information).

The amount of organic matter (SDA) occluded in the zeolite was determined by C, H, N elemental chemical microanalysis in a LECO-CNNS-932 analyzer. Thermogravimetric analyses were performed under oxygen flow (100 mL/min) in an SDT Q600 TA Instruments equipment up to 1000 °C (with a heating rate of 10 °C/min).

**Molecular Mechanics Simulations.** The location and interaction energies of the different imidazolium derivatives in MFI and TON were studied by molecular mechanics simulations, as implemented in the Forcite module in the Materials Studio software.<sup>23</sup> The geometry of the zeolite structures has been kept fixed during all these calculations. Molecular structures and the interaction energies of the organic SDAs with the framework were described with the CVFF forcefield.<sup>24</sup> Periodic boundary conditions (PBC) were applied in all the calculations. The atomic charges for the organic molecules were calculated by the charge-equilibration method,<sup>25</sup> setting the total net molecular charge to +1 (1E3MI) or +2 (for 3BI, 4BI, 5BI, and 6BI). The positive charge of the organic SDA molecules was compensated by the framework using a related version of the uniform charge background method,<sup>26</sup> where the atomic charge for every silicon framework atom was reduced from 0.6 until charge neutrality. Framework oxygen charges were kept fixed to –0.3. These framework charges were used in order to simulate the hydrophobicity of the all-silica ZSM-5 material. We also studied the effect of introducing localized –1 charges on F atoms, with F located in the [4<sup>1</sup>5<sup>2</sup>6<sup>2</sup>] cages of the MFI structure, in the same positions as revealed by XRD in an MFI sample obtained with tetrapropylammonium and fluoride;<sup>27</sup> in this mixed charge-background model, half of the cationic charges were compensated by the presence of F<sup>–</sup> anions (4), and the other half by a uniform charge background on Si atoms (corresponding to 4 SiOH/SiO<sup>–</sup> defects, as experimentally observed, see below). We found exactly the same trend in the interaction energies as with the initial uniform charge-background method (see comparison below), showing that the latter is a good approximation for charge-balancing purposes.

Initially, the molecules were manually docked in the structures in appropriate supercells of the zeolite frameworks under packing values closely similar to those observed experimentally. The most stable location for the SDA molecules was obtained by means of simulated annealing calculations. The interaction energy was calculated by subtracting the energy of the molecules in vacuo to the total energy of the system, and was normalized to energies per unit cell and per Si atom; all the energy values are given in kilocalories per mole (kcal/mol).

**Density Functional Theory Calculations.** To understand the <sup>19</sup>F NMR spectra of the MFI samples observed experimentally, a complementary computational study based on quantum mechanics was performed. Calculations were carried out within the Density Functional Theory (DFT) methodology, using plane-waves as basis set (with a cutoff of 500 eV), and the PBE generalized gradient approximation as functional.<sup>28</sup> Calculation of the NMR parameters were performed with the gauge-including projector augmented-wave method (GIPAW) developed by Pickard and Mauri,<sup>29</sup> as implemented in the CASTEP<sup>30</sup> module in Materials Studio.<sup>31</sup> This computational methodology has been shown to accurately predict the NMR properties of zeolite materials.<sup>32</sup> Dispersion interactions were accounted for through the Grimme dispersion method (DFT+D).<sup>33</sup> The MFI structure with the SDA molecules and F ions was first geometry optimized under this level of theory, and subsequently, the NMR properties were calculated,

obtaining the absolute shieldings of the different nuclei. The chemical shift for a nucleus in a given position ( $\delta(r)$ ) is then defined as:

$$\delta(r) = \sigma_{\text{ref}} - \sigma(r) \quad (1)$$

where  $\sigma(r)$  is the isotropic shielding obtained in the calculations. To compare with the experimental  $^{19}\text{F}$  chemical shifts, we selected a  $\sigma_{\text{ref}}$  of 137 ppm, in such a way that the theoretical and experimental chemical shifts of the most shielded F atom coincide at  $\sim 80$  ppm. Indeed, we are successfully using the same value of  $\sigma_{\text{ref}}$  in other ongoing studies of  $^{19}\text{F}$  NMR properties of other fluorine-containing microporous solids.

## RESULTS AND DISCUSSION

**Zeolite Synthesis.** All the SDAs used in this work consistently produced TON (Table 1), a zeolite that can be

**Table 1. Summary of Synthesis Results**

SDA	H <sub>2</sub> O/SiO <sub>2</sub>	time (days)	phase
1E3MI	8.5	3	TON
		6	TON
		18	TON
		3.5	Amorphous
		5	MFI
	3.5	7	TON + MFI
		17	TON
		19	TON
		3	Dense phase
		13	Amorphous
		4.3	TON
4BI	7.1	1	Amorphous
		3	TON
		6	TON + amorphous
		9	TON
		26	TON
	6.9	2	TON
		5	TON
		4.8	MFI
		5	TON
		4.3	TON
5BI	6.4	4	TON
		8	TON
		1	Amorphous
		8	Amorphous
		15	TON
	6.0	3	TON + amorphous
		6	TON
		12	TON
		4.3	Amorphous+TON
		13	TON

considered as a default structure for pure silica compositions. A default structure<sup>12</sup> may be defined as one that does not require any particularly strong specificity in structure direction and,

thus, may be crystallized using many different organics in a wide range of conditions. Alternatively, one can say that when an SDA fails to display any significant specificity in its structure-direction role, a default structure able to loosely accommodate the organics crystallizes.

In this work, the only hint for a more specific direction among the bis-imidazolium series is displayed by the 4BI cation that, in addition to TON, was also able to produce zeolite MFI when the crystallization was carried out at very high concentration (H<sub>2</sub>O/SiO<sub>2</sub> ratio of 4.8). The fact that a four-methylene spacer produces zeolite MFI is in sharp contrast with previous reports showing that hexamethylene bridges in polyalkylammonium SDAs are generally more adequate to yield this zeolite.<sup>22,34</sup> For polycations with cationic moieties located at channel intersections of MFI and separated by linear alkane spacers, it has been found that 6 methylene spacers apparently closely match the distance between adjacent channel intersections, allowing an optimal fit, while 5 or 7 methylenes may also eventually work.<sup>22,35</sup> This suggests that the two imidazolium rings of each 4BI molecule do not occupy adjacent channel intersections. Interestingly, the singly charged 1E3MI, which can be formally considered as the “monomer” of the 4BI bis-imidazolium, showed a similar structure-direction effect, yielding generally TON, and only when working at very high concentrations (H<sub>2</sub>O/SiO<sub>2</sub> ratio of 3.5) also MFI. Even in those cases, MFI was observed to be metastable and transformed into the more stable TON by Ostwald ripening. It is also worth noting that the crystallization of MFI, and its transformation to TON, is much faster with 4BI than with 1E3MI (Table 1).

The observation that 4BI and 1E3MI may yield MFI or TON depending on the degree of concentration of the synthesis mixture agrees with the general observation, recently termed as the Villaescusa's rule,<sup>36</sup> that silica materials with a lower framework density are favored at more concentrated conditions in fluoride media.<sup>37</sup> Additionally, since the rest of cations used in this work gave no hint of MFI even at high concentration and short crystallization time, apparently a faint but certain structure-direction effect as the one sought exists. This merited, in our opinion, a theoretical investigation, which in turn required a detailed characterization of the obtained materials, specially of the ones crystallized with 4BI and 1E3MI.

**Zeolite Characterization.** Table 2 lists chemical composition details of each kind of SDA-zeolite obtained in this work. The C/N molar ratio of the zeolites is close to the value in the SDA used suggesting that the SDAs are occluded chiefly intact within the zeolites, although there are deviations that suggest decomposition products might also get occluded in certain

**Table 2. Chemical Composition of the Zeolites Obtained in This Work**

SDA	phase	%C	%H	%N	C/N <sup>a</sup>	H/N <sup>a</sup>	empirical formula <sup>b</sup>
1E3MI	MFI	5.1	0.9	1.9	3.1(3.0)	6.6(5.5)	$[\text{C}_6\text{H}_{11}\text{N}_2\text{F}]_{4.4}[\text{SiO}_2]_{96}:5.30\text{H}_2\text{O}$
4BI	MFI	7.5	1.3	3.2	2.7(3.0)	5.6(5.0)	$[\text{C}_{12}\text{H}_{20}\text{N}_4\text{F}_2]_{3.9}[\text{SiO}_2]_{96}:4.50\text{H}_2\text{O}$
1E3MI	TON	4.2	0.8	1.7	2.9(3.0)	6.5(5.5)	$[\text{C}_6\text{H}_{11}\text{N}_2\text{F}]_{0.96}[\text{SiO}_2]_{24}:1.00\text{H}_2\text{O}$
3BI	TON	4.6	0.8	2.2	2.4(2.75)	5.1(4.5)	$[\text{C}_{11}\text{H}_{18}\text{N}_4\text{F}_2]_{0.62}[\text{SiO}_2]_{24}:0.70\text{H}_2\text{O}$
4BI	TON	5.4	1.0	2.2	2.9(3.0)	6.3(5.0)	$[\text{C}_{12}\text{H}_{20}\text{N}_4\text{F}_2]_{0.64}[\text{SiO}_2]_{24}:1.69\text{H}_2\text{O}$
5BI	TON	4.5	0.9	1.9	2.7(3.25)	6.6(5.5)	$[\text{C}_{13}\text{H}_{22}\text{N}_4\text{F}_2]_{0.54}[\text{SiO}_2]_{24}:1.18\text{H}_2\text{O}$
6BI	TON	4.6	0.9	1.7	3.1(3.5)	7.4(6.0)	$[\text{C}_{14}\text{H}_{24}\text{N}_4\text{F}_2]_{0.49}[\text{SiO}_2]_{24}:1.28\text{H}_2\text{O}$

<sup>a</sup>Molar ratio. The theoretical value is given in parentheses. <sup>b</sup>SDA from N analysis assuming the SDA is intact, SiO<sub>2</sub> taken as the TG residue and water derived from the excess H/N ratio (it may actually be water or SiOH defects). The amount of F in 4BI-MFI is derived from the relative intensity of the  $^{29}\text{Si}$  resonances around  $-145$  ppm, assigned to  $[\text{SiO}_{4/2}\text{F}]^-$  units (see text). For the TON zeolites, a significant concentration of connectivity defects is revealed by  $^{29}\text{Si}$  MAS NMR and the amount of F balancing cationic charges is not determined.

cases. This is more conclusively deduced from the  $^{13}\text{C}$  MAS NMR spectra of the materials, which show the expected resonances for the alkyl (50–0 ppm) and aromatic (140–120 ppm) carbons, although, at least in the 3BI-TON sample, additional resonances likely due to decomposition products are also observed (Supporting Information Figure S2). Apparently, trimethylene bridges may provide a reduced stability of doubly charged SDAs, since Lee et al. also reported degradation of trimethylene-bis(trimethylammonium) in conditions comfortably withstood by larger diquats.<sup>14</sup>

The  $^{13}\text{C}$  NMR spectra of 4BI and 1E3MI in MFI or TON zeolites (Figure 1) show a close similarity, as expected due to

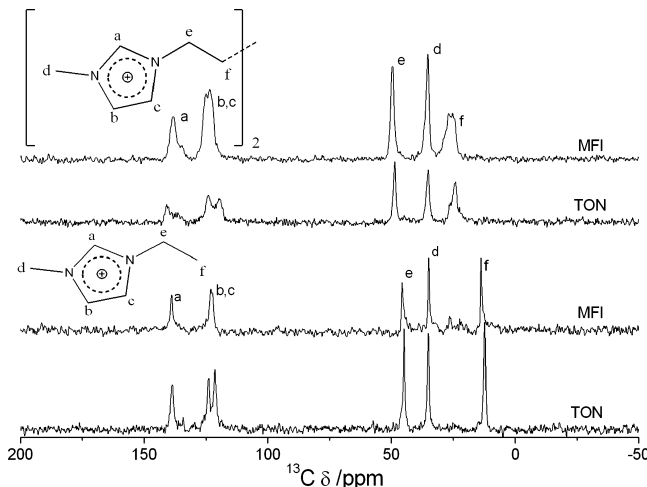


**Figure 1.**  $^{13}\text{C}\{^1\text{H}\}$  CPMAS NMR spectra of as-made TON and MFI zeolites synthesized with 1E3MI (bottom) and 4BI (top).

their similar molecular structure. For both cations, the aromatic carbons at positions 4 and 5 of the imidazolium rings are better resolved in TON than in MFI zeolites, which may point to a wider range of different environments for the imidazolium ring in MFI resulting in broader resonances. Interestingly, the organic contents are much larger in the MFI sample synthesized with 4BI than in the one prepared with 1E3MI (Table 2).

The  $^{29}\text{Si}$  MAS NMR and  $^{29}\text{Si}\{^{19}\text{F}\}$  CP MAS NMR spectra of the MFI as-made materials (Figure 2) evidence a different Si–F

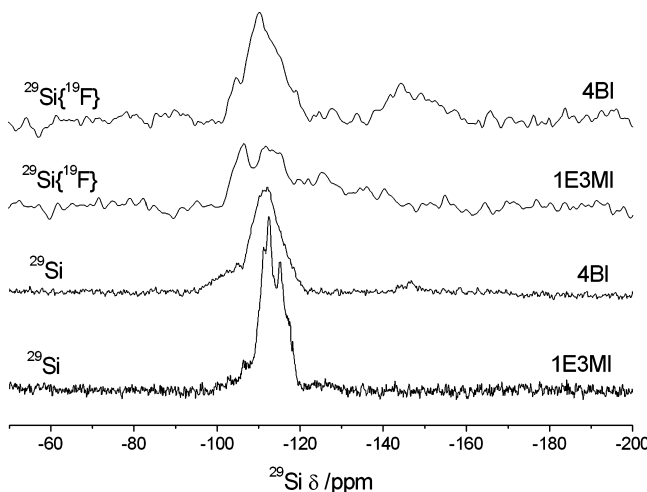


**Figure 2.**  $^{29}\text{Si}$  MAS NMR and  $^{29}\text{Si}\{^{19}\text{F}\}$  CPMAS NMR spectra of the as-made MFI materials.

interaction in the materials prepared with 1E3MI and 4BI. While the most prominent features in the spectra of both materials are the Si Q<sub>4</sub> resonances in the -108/-120 ppm region, a very broad band centered around -125 ppm is observed in 1E3MI-MFI, which is characteristic of Si sites changing their coordination between 4 and 5 ( $[\text{SiO}_{4/2}]$  and  $[\text{SiO}_{4/2}\text{F}]^-$ , respectively), a situation similar to that found in TPA-MFI synthesized in fluoride medium.<sup>38</sup> In contrast, this resonance is absent in the spectrum of 4BI-MFI, which shows instead two sharp and small resonances around -145 ppm, whose relative intensity is sharply increased in the  $^{29}\text{Si}\{^{19}\text{F}\}$  CP MAS NMR spectrum. This is indicative of pentacoordinated  $[\text{SiO}_{4/2}\text{F}]^-$  units which are observed in TPA-MFI only when the dynamic situation described above is frozen at 140 K.<sup>39</sup> A deconvolution of the  $^{29}\text{Si}$  MAS NMR spectrum of 4BI-MFI indicated that around 3.3% of the Si atoms (3.2 Si per unit cell of 96 Si) are involved in  $[\text{SiO}_{4/2}\text{F}]^-$  units. Since, according to CHN analysis, there are almost four doubly charged 4BI cations per unit cell, this suggests that barely half of the cationic charges are compensated by  $[\text{SiO}_{4/2}\text{F}]^-$  units. The  $^{29}\text{Si}$  MAS NMR spectrum also shows that, contrarily to 1E3MI-MFI and the most general case for pure silica zeolites synthesized in fluoride medium, which typically have a very small concentration of defects,<sup>40</sup> the sample crystallized with 4BI contains a significant amount of Q<sub>3</sub> defects evidenced by the broad resonance around -103 ppm (13.6%, or 13.1 SiO<sup>-</sup> or SiOH per unit cell). This suggests that balance of the SDA cationic charges in 4BI-MFI involves both fluoride and SiO<sup>-</sup> and that the total amount of Q<sub>3</sub> largely exceeds (around 4 times) that of SiO<sup>-</sup>. This Q<sub>3</sub> excess is similar to that typically found in silica zeolites prepared in highly basic conditions using cationic SDAs.<sup>41</sup>

As-made TON materials show a strong resonance around -112 ppm due to Q<sub>4</sub> sites together with a weaker one around -102 ppm characteristic of Q<sub>3</sub> (Si-O<sup>-</sup> or Si-OH defects, spectra not shown). There is no clear indication in these spectra of silicon sites interacting with fluoride, although  $^{19}\text{F}$  MAS NMR show resonances in the -75/-76 ppm typical range for  $\text{SiO}_{4/2}\text{F}^-$  in TON.<sup>7</sup>

Figure 3 shows the  $^{19}\text{F}$  MAS NMR spectra of the as-made MFI zeolites. Both samples contain two resonances: one

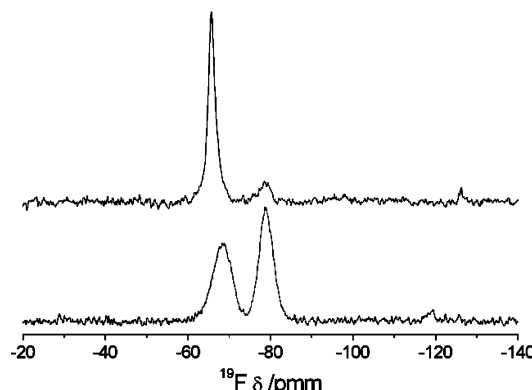


**Figure 3.**  $^{19}\text{F}$  MAS NMR spectra of the as-made 1E3MI-MFI (top) and 4BI-MFI (bottom).

around -66 or -68 ppm (for 1E3MI-MFI and 4BI-MFI, respectively), appears at a chemical shift similar to that observed in TPA-F-MFI (-64 ppm),<sup>39</sup> and the other one is at a higher field (-79 ppm in both cases). In 4BI-MFI, both resonances are broad and have almost exactly the same

intensity, while in 1E3MI-MFI, the resonances are narrower and the intensity of the high field signal is barely 10% of that of the low field one. The existence of these two  $^{19}\text{F}$  resonances, indicative of two different chemical environments for fluoride, sharply contrasts with previous observations in MFI synthesized using TPA and F ions, in which fluoride has been unambiguously located by solid-state NMR techniques in a [4 $^1\text{S}^2\text{6}^2$ ] cavity of the silica framework yielding a single  $^{19}\text{F}$  resonance.<sup>42</sup> The successful application of such NMR techniques requires a very good resolution of crystallographic sites in the  $^{29}\text{Si}\{\text{H}\}$  spectrum which could not be achieved in our sample (Supporting Information Figure S3), probably due to the relatively high concentration of connectivity defects. A structural analysis of 4BI-MFI using single-crystal diffraction is also prevented because of the small crystallite size (in the micrometer range). Attempts to analyze the structure using low resolution powder diffraction lab data failed due to the complexity of the system: the final model described below would contain 106 Si, O, F, C, and N atoms in the asymmetric unit in the topological symmetry, space group *Pnma*, including site occupancies of 1/8 for F, C, and N. Thus, we have studied this issue by DFT calculations (see below).

The presence of SiOH defects in 4BI-MFI is also apparent in its  $^1\text{H}$  MAS NMR spectrum (Figure 4) which shows, in

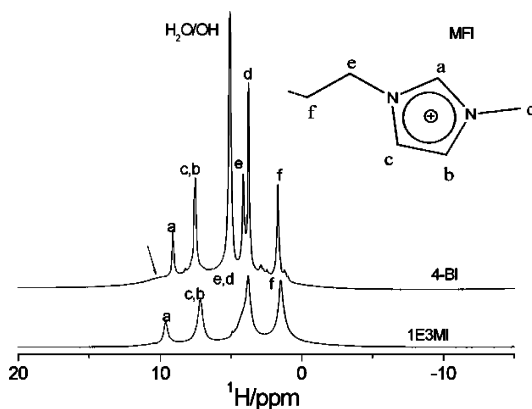


**Figure 4.**  $^1\text{H}$  MAS NMR spectra of MFI zeolites synthesized using 4BI (top) and 1E3MI (bottom). The a–f letters refer to H assignations to C labeled as shown. In the spectrum of 4BI-MFI, a broad band at 10.2 ppm assigned to SiOH hydrogen bonded to charge compensating  $\text{SiO}^-$  groups is marked with an arrow.

addition to the SDA resonances, a broad resonance around 10.2 ppm, assigned to SiOH involved in hydrogen bonds to charge compensating  $\text{SiO}^-$  groups.<sup>41,43</sup> The concentration of silanol groups cannot be reliably determined from this spectrum because of the broad background and the spreading of the intensity in spinning side bands (beyond the chemical shift range shown in Figure 4). Another strong resonance at 5.1 ppm is assigned to  $\text{H}_2\text{O}$  or SiOH in weaker hydrogen bonds.

**Computational Simulations.** To understand the structure-direction behavior of the SDA molecules, a computational study based on molecular mechanics was performed to determine the location and interaction energies of the different SDA cations within the MFI structure. Initially, the same packing values of organic molecules per unit cell as the ones experimentally found were employed. The primitive MFI unit cell was large enough as to enable the study of the SDA molecules under the experimentally observed packing values, without imposing artificial constraints by periodicity.

### 1. Structure-Directing Effect of 4BI in the Synthesis of MFI.

First, we studied the location and interaction energy of 4BI in the MFI structure. Table 3 shows the theoretical organic

**Table 3. Several 4BI-MFI Models Studied by Molecular Mechanics Calculations**

entry	Packing 4BI/u.c.	SDA distribution	imidazolium location	$E^a$
1	2	[010]	intersections	-356
2	2	[010]	no intersections	-347
3	2	[100]	intersections	-349
4	2	[100]	no intersections	-345
5	4	2×[010] + 2×[100]	2× intersections 2× no intersections	-650
6	4	2×[010] + 2×[100]	no intersections	-686

<sup>a</sup>Interaction energy (kcal/mol per u.c.).

contents employed and the distribution and location of the SDA molecules, as well as the interaction energies (in kcal/mol per MFI unit cell). Both the straight [010] and the sinusoidal [100] channels have appropriate dimensions as to host the 4BI molecules. To understand the structural relationship between the MFI topology and the 4BI molecule, we initially studied an organic content of 2 4BI per unit cell, sited in the straight or in the sinusoidal channels; simultaneously, we tried two different locations for the molecules on each type of channel system, with the imidazolium rings in the intersections between the two channel systems or in between the intersections, that is, with the polymethylene bridge sited in the channel intersection (Table 3, entries 1–4 and Supporting Information Figure S4). The energy results indicate that in both types of channel systems, the imidazolium rings are better accommodated in the channel intersections, probably due to the bulky size of the rings and the larger void volume associated with the intersections. In addition, location of the 4BI molecules is energetically preferred in the straight over the sinusoidal channels.

We then increased the organic content to 4 molecules per unit cell, which corresponds to the one experimentally found (3.9). In this case, we have 8 imidazolium rings (2 per molecule), but there are only 4 channel intersections per MFI unit cell. After a set of preliminary calculations, we found two different SDA arrangements that correspond to minima in the potential energy surface (PES), (i) with two of the molecules with the imidazolium rings sited in the intersections and the other two in between them (entry 5 in Table 3, Supporting Information Figure S5), and (ii) with all the imidazolium rings sited out from the intersections, with these being filled by the polymethylene bridges (Table 3, entry 6, Figure 5). Despite the previous finding that the imidazolium rings are better accommodated in the intersections (entries 1 and 3), we observed that, under this higher organic content, a much more stable situation is found when the intersections are occupied not by the imidazolium rings but by the polymethylene bridge (Table 3, entry 6), the energy difference being 36 kcal/mol per unit cell; this is clearly attributable to a better packing between the molecules under this arrangement.

The most stable location of the 4BI molecules within the MFI structure, with the polymethylene bridge in the intersections (entry 6), is shown in Figure 5; the pore volume of the SDA-free MFI structure is also shown to facilitate the visualization of the different channel systems (in transparent blue). Two types of locations of the 4BI molecules (4 molecules per unit cell)

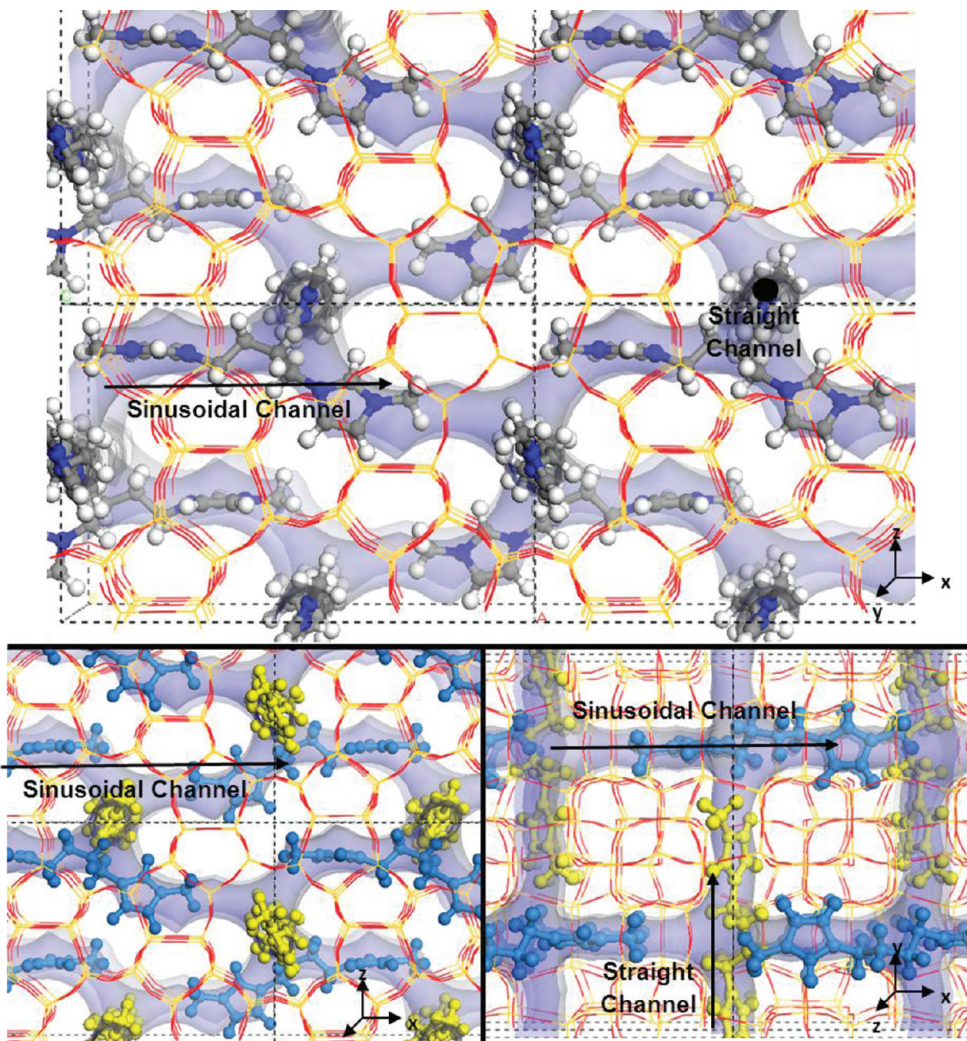


**Figure 5.** (Top) Location of 4BI (4 molecules per unit cell) within the MFI structure (entry 6 in Table 3). (Bottom) The two types of molecular locations are shown in yellow and blue to differentiate them. The pore volume of the SDA-free MFI structure is also displayed in transparent blue.

can be appreciated: two molecules (displayed in yellow in Figure 5, bottom) site along the [010] straight 10MR channels, and the other two are located in the sinusoidal [100] 10MR channels (shown in blue), resulting in a very efficient space-filling of the void volume of the MFI structure.

A detail of the packing between the SDAs is shown in Figure 6. We observe that the dimensions of the 4BI molecule are suitable as to allow for a perfect packing of the molecules in the straight and sinusoidal channels, preventing a steric repulsion between them. Interestingly, if we examine carefully the conformation of the molecules located in the sinusoidal channels (in blue in Figure 5, bottom), we observe that the two imidazolium rings are oriented perpendicular to each other, with the polymethylene bridge located in the intersection with the straight channels, just between two consecutive molecules sited in the straight channels (Figure 6). This particular SDA conformation is a consequence of a better packing under this arrangement, since the most stable conformation of the 4BI molecule in vacuo has the two imidazolium rings parallel to each other, with the energy difference between the two conformations being  $\sim 14$  kcal/mol per molecule (Supporting Information Figure S6). Instead, the molecules sited in the straight channels are located with the two imidazolium rings

roughly parallel to each other (see Figure 6). We should note that the locations found, with the cationic centers in the channels and the polymethylene bridges crossing the channel intersections, are unusual since the opposite situation is typically observed in MFI materials synthesized with other doubly charged SDAs formerly reported, where the cationic moieties, much bulkier than those in our series, must site in the channel intersections.<sup>44</sup>

**2. Structure-Directing Effect of Bis-imidazolium Cations in the Synthesis of MFI as a function of the spacer length.** Once the structure-directing behavior of the 4BI cation was analyzed, we studied the effect of the spacer length on the structure-directing ability of this type of molecules toward the MFI framework. As reported above, the only doubly charged cation that enabled the synthesis of the MFI structure was 4BI; experimental results indicated an organic content of around 3.9 molecules per unit cell. Hence, a packing value of 4 molecules per unit cell was studied for all the bis-imidazolium cations. Table 4 displays the results of the interaction energy for the different SDAs.

The energy results show that, for such organic content, the highest interaction energy is achieved by the 4BI molecule ( $-686$  kcal/mol per unit cell); this is in good agreement with the experimental observation that only this bis-imidazolium

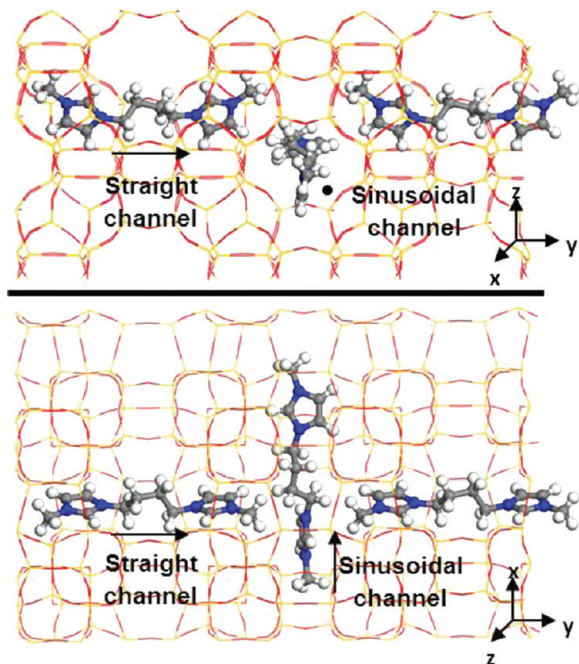


**Figure 6.** Detail of the packing of the 4BI molecules within the MFI structure (entry 6 in Table 3).

cation was found to direct the crystallization of the MFI structure under the experimental conditions tried.

**Table 4. Interaction Energies Calculated by Molecular Mechanics for the Different SDAs in MFI**

SDA	exp. packing	packing used	E. <sup>a</sup>
3BI	-	4	-669 (-6.97)
4BI	3.9	2	-356 (-3.71)
		4	-686 (-7.14)
SBI	-	4	-641 (-6.68)
6BI	-	4	-639 (-6.66)
1E3MI	4.4	4	-302 (-3.15)
		5	-368 (-3.84)
		8	-566 (-5.90)

<sup>a</sup>Interaction energy in kcal/mol per unit cell, and per Si between brackets. These energies were -653 (3BI), -670 (4BI), -630 (SBI), and -627 (6BI) kcal/mol per unit cell when using the mixed charge-background model (see computational details).

A lower interaction energy of -669 kcal/mol was found for the 3BI molecule, suggesting a poorer structure-directing ability of this molecule to direct the crystallization of the MFI structure, that may be even poorer considering its plausible degradation under the synthesis conditions (according to <sup>13</sup>C MAS NMR results, see above and Figure S2), in agreement with the experimental observations. The final location of the molecules is shown in Figure S7, top (Supporting Information). In this case, the dimensions of the molecule do not allow for the efficient packing arrangement achieved by 4BI: the lower interaction energy might be due to the shorter aliphatic chain of this SDA, which is not long enough as to enable a stable accommodation of the imidazolium rings on the sinusoidal channels, as found for 4BI.

An increase of the methylene chain to 5 C atoms leads to a decrease of the interaction energy (-641 kcal/mol), probably due to destabilizing van der Waals short contacts between the

very tightly confined molecules. Despite the larger number of SDA atoms, that in principle should lead to a higher interaction (just taking into account the amount of guest atoms), the interaction energy is lower than with 4BI, clearly indicating that the aliphatic chain of SBI is too large as to allow for a good accommodation of these molecules under this arrangement (Figure S7, middle). Finally, a further increase of the methylene chain to 6 C atoms brings about a further decrease of the interaction energy to -639 kcal/mol, again due to the highly constrained molecules occluded in the confined space of the MFI pore structure (Figure S7, bottom). Such lower interaction energies of these larger SDAs explain the noncrystallization of the MFI structure with these molecules observed in the experimental work.

**3. Structure-Directing Effect of 4BI and 1E3MI in the Synthesis of MFI.** Next, we studied the “monomer” SDA, 1E3MI. In this case, the experimental results showed a lower organic content of 4.4 singly charged molecules per unit cell (equivalent, in terms of N atoms, to 2.2 bis-imidazolium SDAs per unit cell). Accordingly, we studied packings of 4 and 5 molecules per unit cell (Table 4). The different organic content found between this sample and the one obtained with the 4BI SDA makes the interaction energies observed not comparable. For an organic content of 4 molecules per unit cell, we tried two different configurations: with the molecules sited in the straight channels (Figure 7, left) or in the sinusoidal channels (Figure 7, right). Simulated annealing calculations demonstrated that the former configuration is more stable in terms of a stronger interaction with the framework, since the latter case reverted into the former upon simulated annealing (the energy difference was ~25 kcal/mol). The interaction energy (for the system with the molecules in the straight channel) was -302 kcal/mol per unit cell (with an organic content of 4 1E3MI molecules per unit cell).

In an attempt to explain the different organic contents found between the two MFI samples, we additionally studied cases where we loaded 8 1E3MI molecules per unit cell (equivalent to 4BI per unit cell), and 2 4BI molecules per unit cell (equivalent to 4 1E3MI per unit cell); the energy results are collected in Table 4. The presence of 4 4BI molecules per unit cell involves an inclusion of 8 positive charges in the structure that need to be charge-balanced. The <sup>29</sup>Si and <sup>1</sup>H MAS NMR results commented above suggest that barely half of the 4BI cationic charges are balanced by fluoride, while the rest are balanced by SiO<sup>-</sup> connectivity defects. Increasing from 4 N atoms (4 1E3MI or 2 4BI molecules) to 8 N atoms (8 1E3MI or 4 4BI molecules) per unit cell involves an increase in the interaction energy by 264 and 330 kcal/mol per unit cell for 1E3MI and 4BI SDAs, respectively, that is, notably higher for 4BI. The generation of negatively charged structural defects to compensate for the high N content (in the samples with 8 N atoms per unit cell) involves an energy cost, which must be compensated for by the development of strong interactions with the SDAs. The increase of the interaction energy when loading 8 N atoms per unit cell is much higher for 4BI than for 1E3MI, which could explain that only with 4BI molecules this high packing value is experimentally achieved. In the 1E3MI-MFI case, the most stable arrangement corresponds to a loading of 4–5 molecules per unit cell, which prevents the necessity for the formation of charge-compensating defects, in agreement with the <sup>29</sup>Si NMR results.

For the sake of completeness, we also studied by molecular mechanics the location and interaction energies of the SDA

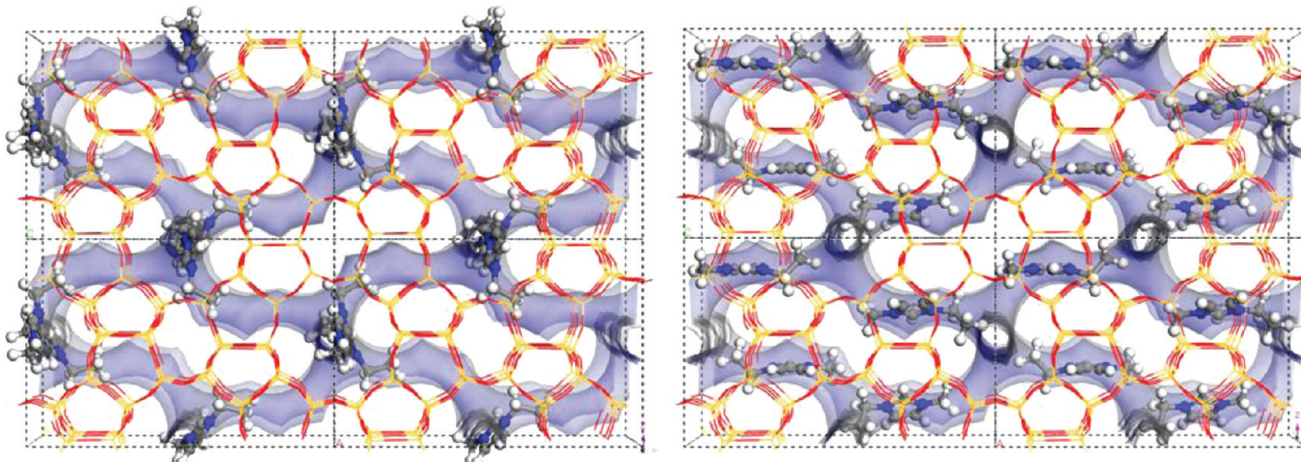


**Figure 7.** Location of 1E3MI molecules in MFI, located within the straight channels (left) or within the sinusoidal channels (right); the latter configuration reverted into the former one upon simulated annealing.

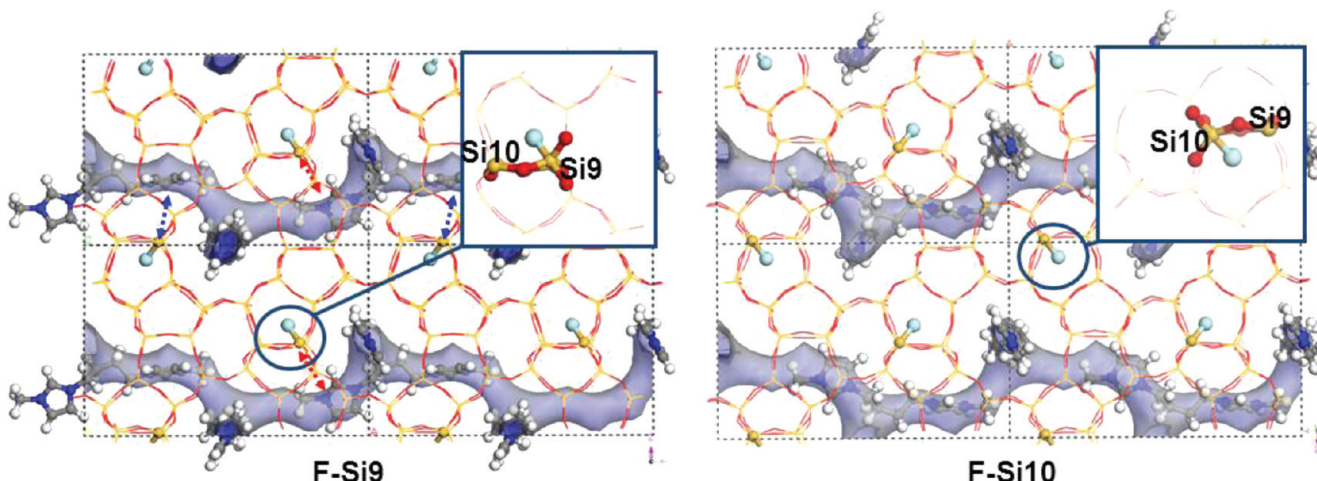


**Figure 8.** DFT-geometry optimized structure of MFI with four 4BI and four F ions in the  $[4^15^26^2]$  cages bonded to Si9 (left) or Si10 (right), and detail of the Si–F environment (insets). Dashed blue and red arrows (left) highlight the two types of interactions of Si–F with the imidazolium rings (see text).

molecules within the TON zeolite (Figure S8 and Table S1 in the Supporting Information). Examination of the location of the molecules within the TON framework indicates that this type of bis-imidazolium molecules are appropriate SDAs for this structure due to their elongated and elliptical molecular shape, enabling a good fitting with the channel topology of the TON structure. In addition, we observed that 3BI developed the strongest interaction with this structure, in line with the nonobservation of MFI with this SDA.

**4. DFT Study of the NMR Properties of MFI Samples.** To understand the signals observed in the  $^{19}\text{F}$  NMR spectra of the MFI samples, we performed a DFT study to calculate the NMR chemical shielding of the F nuclei in the MFI samples obtained with 4BI and 1E3MI. The initial MFI framework with the F ions was obtained from ref 27, where the F counteranions lie in the  $[4^15^26^2]$  cages strongly coordinated to Si9, which belongs to a 4-membered ring (4MR); there are four of these cages per MFI unit cell, and hence 4 F per unit cell. Indeed, it has been proposed that the localization of F close to 4MRs may be related to its role as a templating agent contributing to the stabilization of the structure by enhancing the formation of 4MRs.<sup>15,37</sup> However, apart from the aforementioned Si9 position,

there is another crystallographically nonequivalent Si position which is also part of the 4MR, Si10. Therefore, we performed geometry optimizations and calculated the chemical shielding tensors in 4BI-MFI systems with F bonded to the two types of positions, from which we estimated the chemical shift following eq 1.

Figure 8 shows the MFI structure (after DFT+D geometry optimization) with the 4BI molecules and the F anions (for clarity, only the first half unit cell along the 'b' axis is shown); the location of the template molecules is very similar to the one we found by molecular mechanics calculations (see Figure S9 in the Supporting Information).

The fluoride anion is covalently bonded to a Si atom that has a total coordination number of 5 and displays a nearly perfect bipyramidal geometry, in agreement with the geometry previously calculated for other F-containing silica zeolites.<sup>45</sup> Geometry optimization of the structures with the DFT+D methodology showed a higher stability of F bonded to Si9 positions, the difference being around 11 kcal/mol per unit cell, in line with previous observations by XRD<sup>27</sup> and NMR<sup>42</sup> of F bonded to Si9 in samples obtained with TPA as SDA. Such different stability of F bonded to the two nonequivalent Si

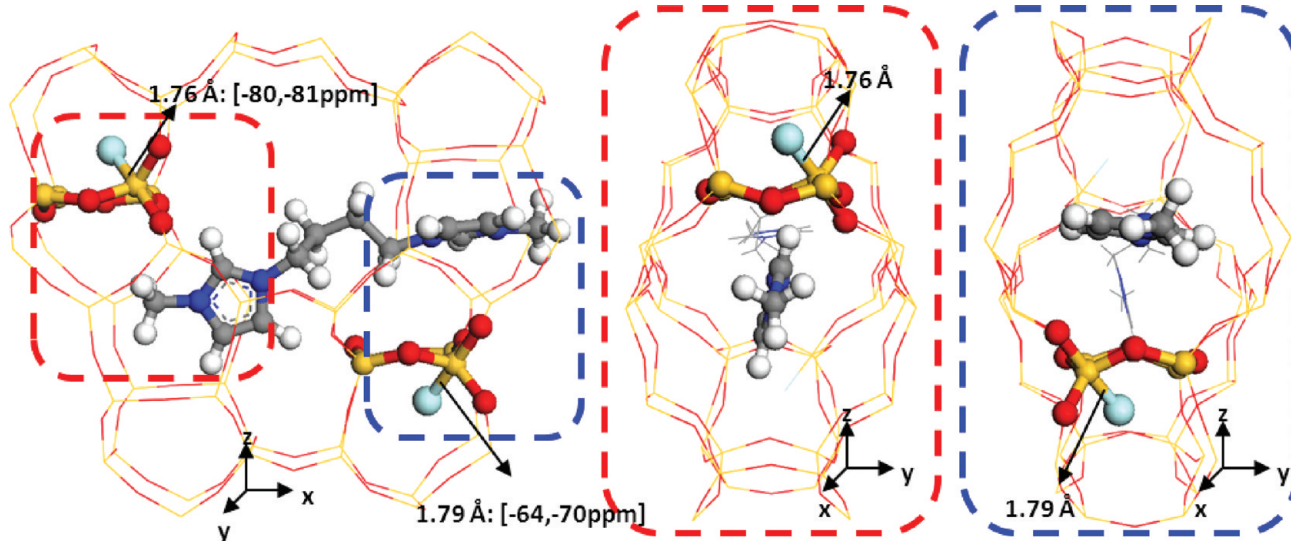


**Figure 9.** Detail of the interaction between F anions and the two imidazolium rings; (left) view along the straight channels; (right) view along the sinusoidal channels; the different Si–F distances associated to each nonequivalent position are displayed. Atoms of the 4MR and F are displayed as balls.

positions in the 4MR could be associated to the more open environment of Si9, which possesses two O atoms in a 10MR, and hence can be more easily distorted to accommodate the trigonal bipyramidal environment brought about by the presence of F (Figure 8, insets). Instead, the two equivalent O atoms in Si10 belong to a 6MR, and are thus more constrained resulting in a higher energy cost to accommodate the new Si environment.

We then analyzed the NMR chemical shielding of the F atoms. Figure 8 (left) shows the final structure of the MFI framework with the F anions and 4 4BI molecules. A careful examination allowed us to recognize two different environments of the F atoms: 2 of them are close to an imidazolium ring of a 4BI molecule sited in a sinusoidal channel with the ring oriented parallel to the 4MR plane (parallel to the *ab* plane, dashed blue arrows in Figure 8, left), and the other 2 interact with the methyl group of the other imidazolium ring of these molecules, with the ring oriented perpendicular to the 4MR plane (perpendicular to the *a* axis, dashed red arrows). We will refer to these two types of orientations of the imidazolium rings with respect to the 4MR as “parallel” and “perpendicular”, respectively. A detail of these two types of environments is shown in Figure 9. F ions close to the “parallel” imidazolium rings (dashed blue rectangles), in which the  $[\text{SiO}_{4/2}\text{F}]^-$  unit interacts more directly with the aromatic  $\pi$  cloud, have slightly longer Si–F distances (1.79 Å) than the F ions interacting with “perpendicular” imidazolium rings, in which the main interaction is with the terminal methyl substituent (1.76 Å, dashed red rectangles). Interestingly, these two different types of F environments give place to theoretical  $^{19}\text{F}$  NMR signals in two different regions: one at lower fields (at -70 and -64 ppm) and another at higher fields (at -80 and -81 ppm), corresponding to the F ions in  $[\text{SiO}_{4/2}\text{F}]^-$  units interacting with the aromatic rings (“parallel” configuration, blue square) or with the methyl substituent (“perpendicular” configuration, red square), respectively. These two different signals predicted by our calculations are in good agreement with the  $^{19}\text{F}$  experimental NMR spectra observed for this sample, with two signals centered at -68 and -79 ppm. Calculation of the chemical shielding tensors of the same system, but removing the molecules sited in the straight channels,

gave similar F environments and chemical shifts (-80, -79, -72, and -69 ppm), thus suggesting that the different F environment is a consequence of the particular location of the 4BI molecules sited in the sinusoidal channels. We should note that the slight difference observed in the low field signals corresponding to F interacting with “parallel” imidazolium rings (-70 and -64 ppm) might be associated to the presence of two Si9 positions in each 4MR, which are topologically equivalent but have an orientation with respect to the “parallel” imidazolium ring that is not chemically equivalent. In contrast, the “perpendicular” orientation of the imidazolium rings makes the two Si9 positions almost chemically equivalent, and so the signals at high field are much more similar, with a difference of less than 1 ppm (-80 and -81 ppm). In sum, these results provide strong support to the computational prediction reached by molecular mechanics about the particular orientation of the 4BI molecules occluded within the sinusoidal channels of the MFI structure.

To confirm the existence of the two types of F environments and that this observation is not a result of a computational artifact during the geometry optimization procedure that traps the system into a local minimum, we repeated the optimization, starting from the final framework structure obtained after optimization with the 4 4BI molecules, with F in the two types of environments, but in the absence of the 4BI molecules. In this case, we found that the geometry optimization led to 4 F ions all with the same Si–F distances and similar  $^{19}\text{F}$  NMR chemical shifts, thus confirming that the presence of the two types of F environments is due to the particular configuration of the 4BI molecules in the sinusoidal channels. The two different chemical environments evidenced by  $^{19}\text{F}$  MAS NMR spectroscopy (Figure 3, bottom) are therefore not due to two topologically distinct locations of fluoride within the MFI framework. Rather, fluoride is covalently bonded to a topologically unique Si site (Si9) giving rise to slightly different  $[\text{SiO}_{4/2}\text{F}]^-$  units by interaction with imidazolium rings in two different orientations within the sinusoidal channels.

If F were bonded to Si10, all the F atoms would show a resonance around -70 ppm (-72, -71, -70, and -67 ppm), and therefore, only one signal should be observed in the

$^{19}\text{F}$  NMR spectrum. Although we cannot discard the presence of this type of F environment by NMR because it would overlap with that of Si9–F interacting with “parallel” imidazolium, the experimental observation of another equally intense resonance at  $-80$  ppm, together with the lower stability of this F environment found by DFT, suggests a minor, if any, presence of this type of Si10–F environment.

The  $^{19}\text{F}$  NMR spectrum of the MFI sample obtained with the monomer molecule, 1E3MI, is dominated by a resonance at  $-66$  ppm, although another signal of lower intensity at  $-79$  ppm is also observed (Figure 3, top). The low field signal ( $-66$  ppm) appears at a different chemical shift from that observed in the 4BI-MFI system (signal at  $-68$  ppm) and, in addition, the shape of the signal is notably different, being almost 3 times narrower. This suggests a different type of F environment for the MFI material obtained with the monomer. Indeed, our calculations by molecular mechanics indicated a higher stability of the 1E3MI molecules when sited on the channel intersections, in sharp contrast to the most stable arrangement of the 4BI molecules; these results are confirmed by DFT, where we also observed a higher stability (by  $\sim 15$  kcal/mol per unit cell) for the 1E3MI sited in the channel intersections. In this case, the existence of a single imidazolium

ring, and so the larger freedom to move, together with the large void volume available in the channel intersections, brings about the existence of a large number of possible different orientations for the 1E3MI molecules sited in the channel intersections.

Therefore, we have studied by DFT many different types of orientations of the 1E3MI cation in MFI: with the imidazolium ring sited in the intersections, oriented parallel or perpendicular to the straight channel direction, and with the ethyl and methyl substituents located in the sinusoidal or in the straight channels (some of the orientations studied are shown in Figure 10). We observed that orientations in which the imidazolium rings are parallel to the straight channels (Figure 10, top) gave calculated  $^{19}\text{F}$  chemical shifts in the range between  $-76$  and  $-81$  ppm. The lowest (more negative) chemical shifts corresponded to orientations in which the molecules, including the ethyl and methyl substituents, were aligned with the straight channels, hence leaving the sinusoidal channels completely free, with a chemical shift around  $-81$  ppm (one of these orientations is displayed in Figure 10, top-left). These molecular orientations could then be associated to the low-intensity experimental signal found at  $-79$  ppm. Inclusion of the ethyl substituent in the sinusoidal channels, both with the imidazolium ring parallel

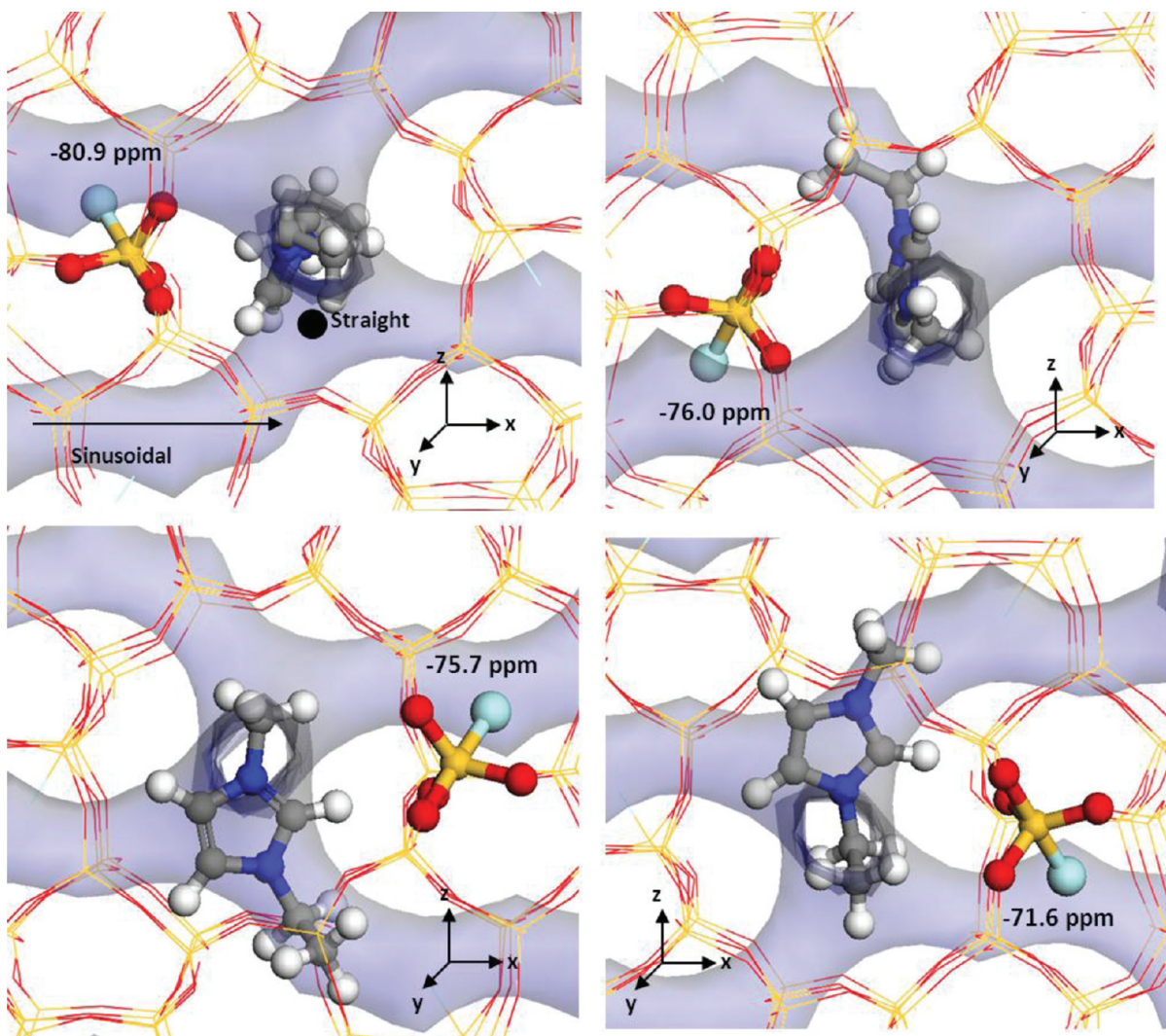


**Figure 10.** Some of the different 1E3MI orientations tried in the DFT+D calculations, and the corresponding  $^{19}\text{F}$  NMR chemical shifts found for the associated F anions.

(Figure 10, top-right) or perpendicular (Figure 10, bottom-left) to the straight channels involved a shift of the resonance toward lower fields (around  $-76$  ppm).

The lowest field resonance we found, and so the closest to the experimental signal of  $-66$  ppm, corresponded to the orientation in which the methyl substituents were sited in the sinusoidal channels, and the ethyl groups aligned with the straight channels (Figure 10, bottom-right), giving a chemical shift of  $-71.6$  ppm. Although closer to the experimental signal of  $-66$  ppm, there is still a difference of  $5$  ppm between the experimental and calculated chemical shifts.  $^{29}\text{Si}$  MAS NMR spectroscopy (Figure 2) demonstrates that fluoride is involved in a dynamic motion at room temperature, jumping to coordinate with different silicon atoms in 1E3MI-MFI (as opposed to the 4BI-MFI case). It has been shown by variable temperature multinuclear MAS NMR that this kind of dynamic motion of fluoride in TPA-F-MFI can be frozen by lowering the temperature to  $140$  K, and that this is accompanied by a change of the  $^{19}\text{F}$  chemical shift of  $6$  ppm to higher field ( $-63.9$  ppm at room temperature,  $-69.9$  ppm at  $140$  K).<sup>39</sup> A similar effect, in sign and magnitude, was also found for zeolites IFR and SST, where F is involved in a similar dynamic situation.<sup>39</sup> Thus, we propose that the main orientation of 1E3MI in MFI is that shown in Figure 10, bottom-right, with the imidazolium ring in the channel intersections and the methyl and ethyl substituents pointing toward the sinusoidal and straight channels, respectively, giving rise to a chemical shift of  $-71.6$  ppm (calculated,  $0$  K) that would likely change several parts per million to lower field at room temperature (experimental,  $-66$  ppm) due to dynamic motion effects of the anion. However, we note that, in the case of the 1E3MI cation, due to the differences observed and the large number of molecular orientations possible, the proposed assignment of the F resonance is tentative.

We should finally note that the signal observed at  $-79$  ppm, apart from the aforementioned assignment to molecules within the straight channels, could also be due to 1E3MI molecules sited within the sinusoidal channels rather than in the intersections, despite their lower stability found by molecular mechanics and DFT, since some of the orientations tried in this new location gave theoretical signals close to  $-80$  ppm. Such lower stability would explain the low intensity experimentally observed.

## CONCLUSIONS

Our synthesis results using bis-(methylimidazolium) SDAs with 3–6 methylene bridges show that a minor length-specific, structure-direction effect occurs only for the four-methylene spacer. The crystallization field is dominated by a “default structure” (TON) and the only departure from this affords the crystallization of MFI. This zeolite may be generally considered as a default structure also, since it is not highly demanding of a specific structure direction, but here is metastable with respect to TON and shows a very narrow crystallization window (low water content, short crystallization time). With this in mind, it is surprising that, nonetheless, there appears to be a particularly preferred location of the charged imidazolium rings in the MFI structure that actually crystallizes, as deduced not only by molecular mechanics simulations but also by the fact that the only spacer affording MFI contains just four methylene groups, and thus has a distance too short between charges to span two channel intersections; the imidazolium rings are thus located out of the channel intersections. We conclude the

crystallization of MFI with 4BI is the result of a subtle structure direction afforded by the adequate length of the cation and the very high organic content that can be achieved in highly concentrated conditions following Villaescusa’s rule. However, considering the very high charge density in 4BI-MFI and the concomitant existence of a high concentration of  $\text{Q}_3$  defects, this would not be possible without a rather strong host–guest stabilization. Our calculations suggest indeed that the charge separation in 4BI affords a strong cation–anion interaction for both imidazolium rings of each molecule in the sinusoidal channels with the same structural motif of the zeolite framework. At the same time, as this location does not block the channel intersections, it affords a high organic loading in the straight channels.

Leaving the 3BI cation aside, because of its lower stability, the 4BI SDA is the one with a higher charge density among those tested, but its very high loading in MFI does not lead to an increased occlusion of fluoride anions. Rather, fluoride is occluded in its usual location in fluoride MFI samples: inside the  $[4^1\text{S}^26^2]$  cavities and covalently bonded to Si9, which presents a trigonal bipyramidal coordination geometry. Since there are only 4 such cavities in MFI,  $\text{SiO}^-$  defects are needed for charge balance. These are accompanied by additional  $\text{SiOH}$  groups (in around 3 times the amount of  $\text{SiO}^-$ ) which participate in moderately strong hydrogen bonds to the charged silanolate. Thus, the MFI sample prepared with 4BI can be regarded as a notable hybrid between a defect-free silicalite prepared by the fluoride route and a defective silicalite prepared at high alkali conditions. From our calculations, fluoride must concentrate in the silica walls surrounding the sinusoidal channels, which would be defect free, while silanols would tend to reside on the linear channel. This would give rise to differentiated hydrophobic/hydrophilic regions inside each crystal.

Two different configurations of each imidazolium ring of 4BI in MFI with regard to the  $[4^1\text{S}^26^2]$  cavities, all of which are occupied by fluoride, give rise to two distinct resonances in the  $^{19}\text{F}$  MAS NMR spectrum, which arise from the different interaction of the  $[\text{SiO}_{4/2}\text{F}]^-$  units with the aromatic cloud and the methyl substituent of the imidazolium ring, as shown by DFT calculations. The different configurations of the imidazolium rings are not a consequence of the interaction with F but of the optimal conformation adopted by the cation, since they appear even in molecular mechanics calculations without occluded fluoride. While 1E3MI may be considered as half a 4BI cation, it is surprising that their respective loadings in MFI are almost the same, so the synthesis of 1E3MI occurs despite a poor space filling of the cavities available and with no connectivity defects. In addition, despite their similar molecular structure, the locations of the two molecules within the MFI framework are sharply different: 1E3MI locates with the imidazolium rings in the channel intersections, while 4BI accommodates the polymethylene bridges in such intersections.

## ASSOCIATED CONTENT

### S Supporting Information

$^1\text{H}$  NMR of SDAs in solution, details of multinuclear MAS NMR, additional  $^{13}\text{C}\{^1\text{H}\}$  and  $^{29}\text{Si}\{^1\text{H}\}$  CPMAS NMR, additional molecular mechanics results for MFI zeolite, study of structure direction of all the SDA toward TON zeolite, comparison of molecular mechanics and DFT location of 4BI in MFI. This material is available free of charge via the Internet at <http://pubs.acs.org>.

## AUTHOR INFORMATION

### Corresponding Author

macamblor@icmm.csic.es

### Notes

The authors declare no competing financial interest.

## ACKNOWLEDGMENTS

Financial support by the Spanish CICYT, MAT2009-09960 is gratefully acknowledged. A.R. thanks CSIC for a JAE-predoc fellowship. L.G.-H. acknowledges the Spanish Minister of Science and Innovation for a Juan de la Cierva contract. Accelrys is acknowledged for providing the software, and Centro Técnico de Informática-CSIC for running the calculations.

## REFERENCES

- (1) Gies, H.; Marler, B. *Zeolites* **1992**, *12*, 42.
- (2) Davis, M. E.; Lobo, R. F. *Chem. Mater.* **1992**, *4*, 756. Lobo, R. F.; Zones, S. I.; Davis, M. E. *J. Inclusion Phenom. Mol. Recognit. Chem.* **1995**, *21*, 47.
- (3) Koelman, C. M.; Li, Y. S.; Freeman, C. M.; Levine, S. M.; Hwang, M. J.; Maple, J. R.; Newsam, J. M. *J. Phys. Chem.* **1994**, *98*, 12911.
- (4) Lewis, D. W.; Freeman, C. M.; Catlow, C. R. A. *J. Phys. Chem.* **1995**, *99*, 11194.
- (5) Baerlocher Ch.; McCusker, L. B. Database of Zeolite Structures: <http://www.iza-structure.org/databases/> (accessed Feb 2012).
- (6) Zicovich-Wilson, C. M.; San-Román, M. L.; Camblor, M. A.; Pascale, F.; Durand-Niconoff, J. S. *J. Am. Chem. Soc.* **2007**, *129*, 11512.
- (7) Zicovich-Wilson, C. M.; Gándara, F.; Monge, A.; Camblor, M. A. *J. Am. Chem. Soc.* **2010**, *132*, 3461.
- (8) Daniels, R. H.; Kerr, G. T.; Rollmann, L. D. *J. Am. Chem. Soc.* **1978**, *100*, 3097.
- (9) Dodwell, G. W.; Denkewicz, R. P.; Sand, L. B. *Zeolites* **1985**, *5*, 153.
- (10) Casci, J. L. *Stud. Surf. Sci. Catal.* **1986**, *28*, 215.
- (11) Casci, J. L.; Stewart, A. *Eur. Pat.* 377291, 1990.
- (12) Moini, A.; Schmitt, K. D.; Valyocsik, E. W.; Polomski, R. F. *Zeolites* **1994**, *14*, 504.
- (13) Hong, S. B.; Min, H. K.; Shin, C. H.; Cox, P. A.; Warrender, S. J.; Wright, P. A. *J. Am. Chem. Soc.* **2007**, *129*, 10870. Hong, S. B.; Lear, E. G.; Wright, P. A.; Zhou, W.; Cox, P. A.; Shin, C.-H.; Park, J.-H.; Nam, I.-S. *J. Am. Chem. Soc.* **2004**, *126*, 5817. Hong, S. B. *Catal. Surv. Asia* **2008**, *12*, 131. Lee, S. H.; Lee, D. K.; Shin, C. H.; Park, Y. K.; Wright, P. A.; Lee, W. M.; Hong, S. B. *J. Catal.* **2003**, *215*, 151. Lee, S. H.; Shin, C. H.; Hong, S. B. *Chem. Lett.* **2003**, *32*, 542.
- (14) Lee, S. H.; Shin, C. H.; Yang, D. K.; Ahn, S. D.; Nam, I. S.; Hong, S. B. *Microporous Mesoporous Mater.* **2004**, *68*, 97.
- (15) Villaescusa, L. A.; Camblor, M. A. *Recent Res. Dev. Chem.* **2003**, *1*, 93.
- (16) Guth, J. L.; Kessler, H.; Caullet, P.; Hazm, J.; Merrouche, A.; Patarin, J. In *Proceedings from the Ninth International Zeolite Conference: Montreal 1992*; von Ballmoos, R., et al., Eds; Butterworth-Heinemann: Boston, MA, 1993; p 215.
- (17) Caullet, P.; Guth, J. L.; Hazm, J.; Lamblin, J. M.; Gies, H. *Eur. J. Solid State Inorg. Chem.* **1991**, *28*, 345.
- (18) Bull, I.; Villaescusa, L. A.; Teat, S. J.; Camblor, M. A.; Wright, P. A.; Lightfoot, P.; Morris, R. E. *J. Am. Chem. Soc.* **2000**, *122*, 7128.
- (19) Arranz, M.; Pérez-Pariente, J.; Wright, P. A.; Slawin, A. M. Z.; Blasco, T.; Gómez-Hortigüela, L.; Corà, F. *Chem. Mater.* **2005**, *17*, 4374.
- (20) Díaz-Cabañas, M. J.; Camblor, M. A.; Liu, Z.; Ohsuna, T.; Terasaki, O. *J. Mater. Chem.* **2002**, *12*, 249.
- (21) Caullet, P.; Paillaud, J. L.; Mathieu, Y.; Bats, N. *Oil Gas Sci. Technol.* **2007**, *62*, 819.
- (22) Jackowski, A.; Zones, S. I.; Burton, A. W. *Stud. Surf. Sci. Catal.* **2008**, *174*, 111. Jackowski, A.; Zones, S. I.; Hwang, S. J.; Burton, A. W. *J. Am. Chem. Soc.* **2009**, *131*, 1092.
- (23) Force Module. *Materials Studio 5.5*; Accelrys, Inc.: San Diego, CA, 2011.
- (24) Dauger-Osguthorpe, P.; Roberts, V. A.; Osguthorpe, D. J.; Wolff, J.; Genest, M.; Hagler, A. T. *Proteins: Struct., Funct., Genet.* **1988**, *4*, 21.
- (25) Rappe, A. K.; Goddard, W. A. III. *J. Phys. Chem.* **1995**, *95*, 3358.
- (26) De Vita, A.; Gillan, M. J.; Lin, J. S.; Payne, M. C.; Stich, I.; Clarke, J. L. *Phys. Rev. B* **1992**, *46*, 12964.
- (27) Aubert, E.; Florence, P.; Souhassou, M.; Petříček, V.; Lecomte, C. *J. Phys. Chem. B* **2002**, *106*, 1110.
- (28) Perdew, J. P.; Burke, K.; Ernzerhof, M. *Phys. Rev. Lett.* **1996**, *77*, 3865.
- (29) Pickard, C. J.; Mauri, F. *Phys. Rev. B* **2001**, *63*, 245101.
- (30) Clark, S. J.; Segall, M. D.; Pickard, C. J.; Hasnip, P. J.; Probert, M. J.; Refson, K.; Payne, M. C. Z. *Kristallogr.* **2005**, *220*, 567.
- (31) CASTEP Module. *Materials Studio 5.5*; Accelrys, Inc.: San Diego, CA, 2010.
- (32) Profeta, M.; Mauri, F.; Pickard, C. J. *J. Am. Chem. Soc.* **2003**, *125*, 541.
- (33) Grimme, S. *J. Comput. Chem.* **2006**, *27*, 1787.
- (34) Beck, L. W.; Davis, M. E. *Microporous Mesoporous Mater.* **1998**, *22*, 107.
- (35) Bonilla, G.; Díaz, I.; Tsapatsis, M.; Jeong, H. K.; Lee, Y.; Vlachos, D. G. *Chem. Mater.* **2004**, *16*, 5697.
- (36) Camblor, M. A.; Hong, S.B. In *Porous Materials*; Bruce, D. W., O'Hare, D., Walton, R. I., Eds.; John Wiley & Sons: Chichester, 2010; pp 265–325.
- (37) Camblor, M. A.; Villaescusa, L. A.; Díaz-Cabañas, M. J. *Top. Catal.* **1999**, *9*, 59.
- (38) Koller, H.; Wölker, A.; Eckert, H.; Panz, C.; Behrens, P. *Angew. Chem., Int. Ed. Engl.* **1997**, *36*, 2823.
- (39) Koller, H.; Wölker, A.; Villaescusa, L. A.; Díaz-Cabañas, M. J.; Valencia, S.; Camblor, M. A. *J. Am. Chem. Soc.* **1999**, *121*, 3368.
- (40) Chézeau, J. M.; Delmotte, L.; Guth, J. L.; Soulard, M. *Zeolites* **1989**, *9*, 78.
- (41) Koller, H.; Lobo, R. F.; Burkett, S. L.; Davis, M. E. *J. Phys. Chem.* **1995**, *99*, 12588.
- (42) Fyfe, C. A.; Brouwer, D. H.; Lewis, A. R.; Chézeau, J. M. *J. Am. Chem. Soc.* **2001**, *123*, 6882.
- (43) Shantz, D. F.; auf der Günne, J. S.; Koller, H.; Lobo, R. F. *J. Am. Chem. Soc.* **2000**, *122*, 6659.
- (44) Beck, L. W.; Davis, M. E. *Microporous Mesoporous Mater.* **1998**, *22*, 107.
- (45) Attfield, M. P.; Catlow, C. R. A.; Sokol, A. A. *Chem. Mater.* **2001**, *13*, 4708.